JOURNAL OF MATERIALS SCIENCE 33 (1998) 4297–4305

Sinterability of commercial 8 mol % yttria-stabilized zirconia powders and the effect of sintered density on the ionic conductivity

I. R. GIBSON*
Department of Chemistry, University of Aberdeen, Meston Walk, Aberdeen AB24 2UE, UK
E-mail: I.R. Gibson@qmw.ac.uk

G. P. DRANSFIELD‡
Tioxide Specialties Ltd, Haverton Hill Road, Billingham, Cleveland TS23 1PS, UK

J. T. S. IRVINE
School of Chemistry, University of St Andrews, St Andrews, Fife KY16 9ST, UK

The sintering behaviour of a number of commercially produced 8 mol % yttria-stabilized zirconia powders has been studied. The effect of different sintering regimes on the density and microstructure of the sintered ceramic was determined using density measurements, scanning electron microscopy (SEM) and dilatometry. The chemical homogeneity, particle size and the morphology of the as-received powder were related to the sintering behaviour of the different commercial powders. Powders prepared via a route which involved a spray-drying step sintered more readily than those prepared without a spray-drying step. Plasma-derived powders did not sinter to as high an apparent density as co-precipitated powders. The effect of sample density on the ionic conductivity of sintered YSZ ceramics was studied using a.c. impedance spectroscopy. This technique allowed separation of the bulk and grain-boundary components, enabling clear intepretation of the effects of sample porosity of the conduction pathways. Ceramics prepared from the three different powders achieved a bulk ionic conductivity of $\sim 16\ S\,cm^{-1}$ at 1000 °C for sintered densities of 95% or greater. The results obtained are compared to values reported for a variety of other commercial powders. © *1998 Kluwer Academic Publishers*

1. Introduction

The excellent high-temperature ionic conductivity of 8 mol % yttria-stabilized zirconia (YSZ) has resulted in it being the material chosen as the electrolyte in solid oxide fuel cells (SOFC). The generation of electricity utilizing SOFCs offers both high conversion efficiency and low environmental contamination, hence SOFC development has been an area of considerable activity and the technology is now approaching commercial viability [1]. In order to improve efficiency, the properties of each component of the SOFC must be optimized. For YSZ electrolytes, the electrical and mechanical properties can be enhanced by preparing YSZ ceramics that have high densities and small grain sizes after sintering. To achieve such a high sintered density, ultrafine powders with a narrow size distribution are required [2] and advanced powder production can allow near theoretical densities to be achieved at progressively lower temperatures [3].

The effect of sample density on the ionic conductivity of YSZ has been studied [4–6]; for high levels of porosity, >10%, a large decrease in conductivity was observed. The presence of pores impairs the conduction path between grains, lowering the conductivity [3]. The attainment of a fully dense ceramic is desired to achieve maximum conductivity. Consequently, recent commercial materials research has focused on producing ultrafine yttria-stabilized zirconia powders which sinter to a high density.

In this study, the sintering behaviour of three different commercial YSZ powders has been investigated. The results were compared to values obtained for other commercial YSZ powders. The influence of sintered density upon the electrical properties of the sintered YSZ ceramics has been investigated.

*Present address: IRC in Biomedical Materials, Queen Mary and Westfield College, Mile End Road, London E1 4NS, UK.
‡Present address: Solaveil ICI Performance Chemicals, Unit 5, Pease Road, Northwest Industrial Estate, Peterlee, County Durham, SR8 2RD, UK.

2. Experimental procedure

2.1. Materials

Three different commercial powders were studied. Powder A was an 8 mol % yttria–zirconia produced by a coating technique and Powder B was an 8 mol % yttria–zirconia prepared by a co-milling technique (both prepared by Tioxide Specialties Ltd, UK) [8]. The preparation of Powders A and B involved the use of a plasma-derived zirconia [8]. Powder C was an 8 mol % YSZ co-precipitated powder produced by Tosoh Corporation, Japan. Powder C is the YSZ used most commonly in SOFC research.

2.2. Powder characterization

The as-received powders were characterized using surface area analysis (BET), particle size analysis and scanning electron microscopy (SEM).

2.3. Powder sinterability

All the powders were used as-received. Powders were uniaxially pressed at 20–150 MPa, using cylindrical 13 and 25 mm dies (Graseby Specac Ltd, UK). The green bodies were sintered in air using a muffle furnace (Carbolite, UK). A typical sintering regime involved a heating/cooling rate of 10 °C min^{-1}, a pre-sinter dwell at 1000 °C for 60 min and a sintering dwell at 1500 °C of 120 min. Initial experiments showed that varying the heating rate and increasing the sintering time did not affect the sintered densities of the three materials.

Green-body and sintered densities were typically obtained from the mass and geometric dimensions of the discs. Samples mass was measured to $\pm$ 0.1 mg and sample radius, r, and thickness, t, to $\pm$ 0.02 mm. Density measurements by the water immersion technique were made and the results compared to values determined by dimension measurements. The water immersion technique is accurate only when samples have densities $>95\%$, as lower-density samples may allow water to enter the pores; for this reason the density of green-body or poorly sintered samples could not be measured using the water immersion technique. All densities were expressed as a percentage of the theoretical density (5.958 g cm^{-3}) [9].

A Netzsch 402 E Dilatometer was used to compare the sintering of the different yttria–stabilized zirconias. A typical analysis involved heating at 10 °C min^{-1} from room temperature to 1000 °C, holding for 20 min, heating at 10 °C min^{-1} to 1500 °C, holding for 120 min, then cooling at 10 °C min^{-1} to room temperature. Dilatometry analysis allowed the activation energy of sintering to be calculated.

An ISI-SS440 scanning electron microscope (SEM) was used to examine the microstructure of sintered samples. The sintered discs were polished to a 1 μm finish, then chemically etched by immersing in HF for 15–30 min. From the scanning electron micrographs, grain sizes could be determined and the distribution of grain sizes deduced. Average grain sizes were determined using the intercept method [10].

2.4. Conductivity measurements

Platinum electrodes were applied as organic pastes to the faces of the YSZ disc and fired briefly at 1000 °C to remove the organics. Two terminal a.c. impedance measurements were performed using a Hewlett Packard HP4192 impedance analyser. An a.c. voltage of 0.1 V was applied to the sample, over a frequency range of 100 Hz to 13 MHz, with ten measurements being made for every decade increase in frequency. Measurements were made in air, over a temperature range of 300–1000 °C. Data were corrected for sample geometry and complex impedance plots allowed conductivities (Ω^{-1} cm^{-1}) and geometric capacitances (F cm^{-1}) to be calculated [11].

3. Results and discussion

3.1. Powder characterization

The surface areas (BET) and particle sizes (particle size analysis) of the three as-received powders are presented in Table I. The surface areas vary significantly, with Powder A having the highest and Powder B the lowest surface area. The results of the particle size analysis listed in Table I indicate that the size of the powder particles in Powders A and C are comparable, whereas Powder B consists of larger powder particles with a much wider size distribution than observed for Powders A and C. This is illustrated more clearly by observing the powders using scanning electron microscopy; scanning electron micrographs of Powders A, B and C are shown in Fig. 1a, b and c, respectively. Powders A and C both consist of highly spherical powder particles which have a wide range of diameters. Each spherical powder particle appears to consist of an agglomeration of smaller crystallites. The minimum to maximum particle sizes observed in Figs. 1a and c and 5–55 μm and 10–100 μm, respectively. Powder B consists of very irregular-shaped powder particles with a size range of between 5 and >400 μm, as observed from Fig. 1b. Part of the production processes used to prepare Powders A and C was the spray-drying of the powders which can result in very spherical powder particles [12]. The preparation of Powder B did not involve spray-drying.

3.2. Powder sinterability

3.2.1. Effect of sintering temperature and time

The three YSZ powders were compacted at 80 MPa using a 13 mm die and sintered at temperatures

TABLE I Results of surface area and particle size analysis of Powders A, B and C ($d(0.1)$, $d(0.5)$ and $d(0.9)$ refer to the measured particle size, or diameter, of 10%, 50% and 90% of the powder particles

Powder	Surface Area (m^2/g)	Particle Size (μm) $d(0.1)$	$d(0.5)$	$d(0.9)$
Powder A	17	24	39	102
Powder B	4	24	125	256
Powder C	11	32	54	90

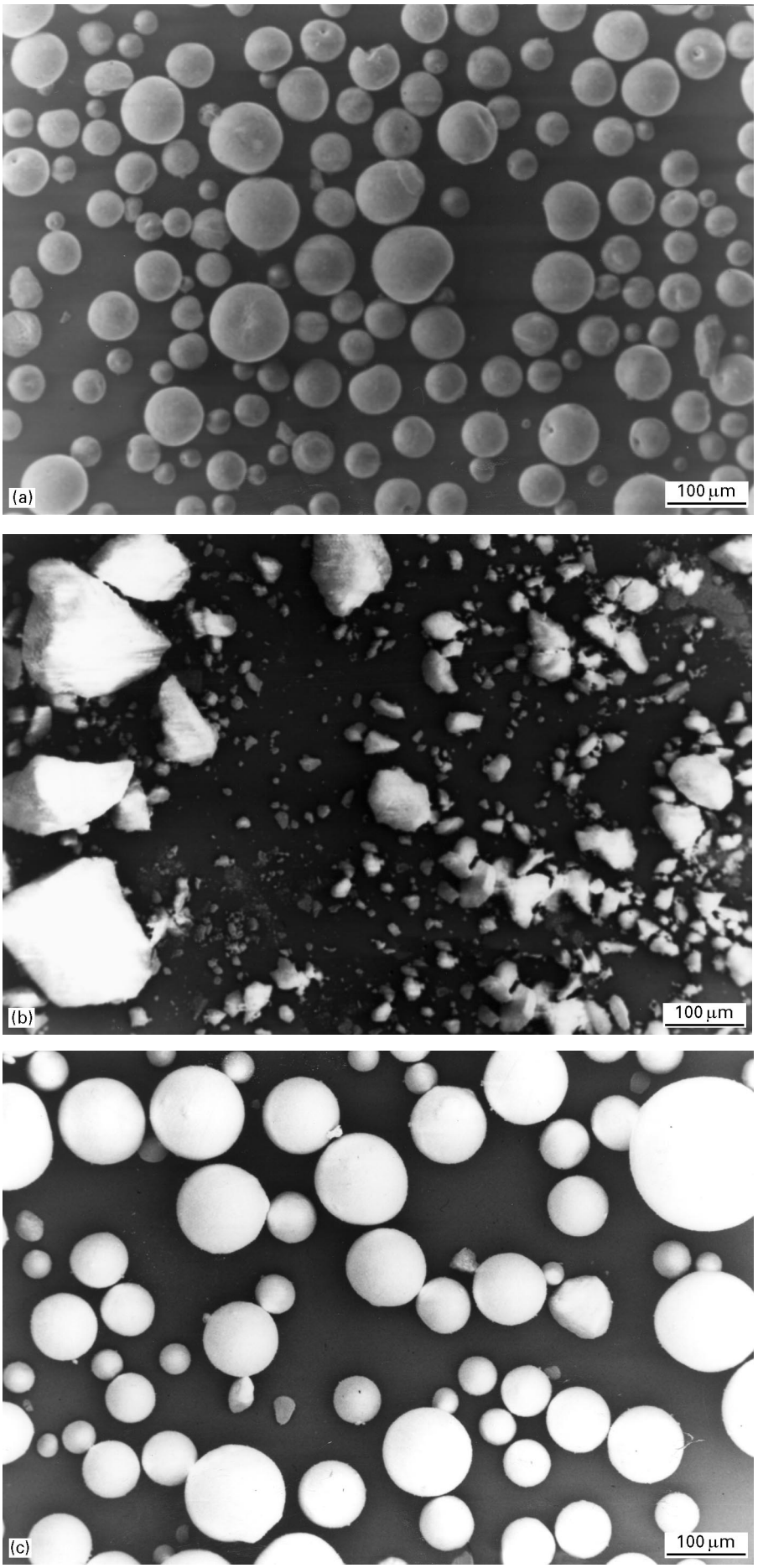

Figure 1 Scanning electron micrographs of (a) Powder A, (b) Powder B and (c) Powder C which illustrate powder morphology and size

between 1000 and 1500 °C for 2 h. The sintered densities were measured using geometric dimensions (for low-density samples) and the water immersion method (for high-density samples) and the results, expressed as a percentage of the theoretical density [9] were plotted against sintering temperature, Fig. 2. Each sample produced a similar-shaped sigmoidal curve. On low-temperature sintering, 1000–1100 °C, the densities were low and not significantly greater than the green densities. Powder B appeared to have the highest density at this stage, suggesting a more efficient packing of the compacted powder particles.

Between 1100 and 1300 °C, a large change in the sintered density of all three materials occurred. A major difference was observed, however, in the temperature at which each powder started to densify. Powder C showed a rapid increase in density at ~1100 °C, whereas a further increase of ~20 °C was required before Powder A showed the same rapid increase; the density of Powder B did not increase until 1150–1175 °C. This difference continued between 1100 and 1300 °C and the temperatures at which samples approached almost full density, e.g. 95%, varied considerably: Powder C at ~1275 °C, Powder A at ~1300 °C.

From 1300–1500 °C, the increase in sintered density was small (2–5%). Powder C sintered to almost full density (99.7%) at 1500 °C, while Powders A and B achieved maxima of 98.5% and 98.2%, respectively.

3.2.2. Powder compaction

The effects of powder compaction on the green and sintered densities of the three materials were studied. Previously, samples were compacted at 80 MPa using a 13 mm die. The effect of varying the compaction pressure from 20–140 MPa, using a 25 mm die, was examined.

Fig. 3a shows the compaction curve, green density (% theoretical) versus log(compaction pressure), for Powders A and B; Fig. 3b is the plot obtained for Powder C, with results obtained for a commercial co-precipitated Y-TZP (Tosoh TZ-2Y) by Theunissen [13] included for comparison. Powdered A and B had

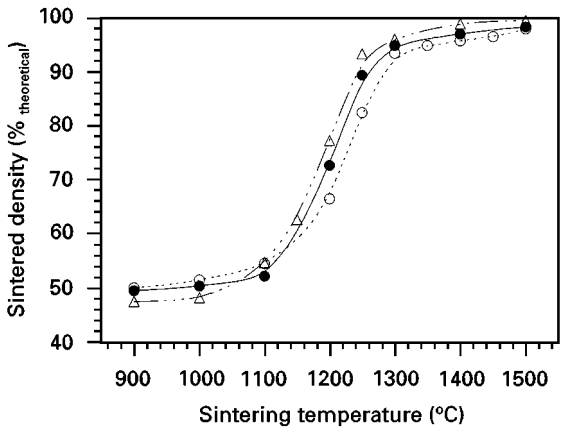

Figure 2 The effect of sintering temperature on the sintered density, expressed as a percentage of the theoretical density, of compacts of Powders (●) A, (○) B and (△) C.

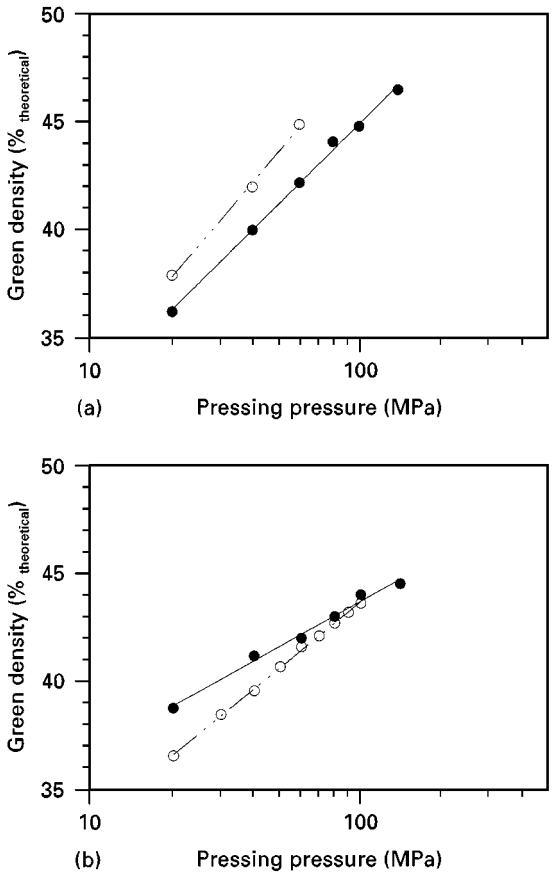

Figure 3 Compaction curves showing the effect of compaction pressure on the green densities, expressed as a percentage of the theoretical density, of compacts of (a) Powders (●) A and (○) B, and (b) (●) Powder C and (○) a commercial co-precipitated Y-TZP (Tosoh TZ-2Y) [13].

gradients *m*, of 14 and 16, respectively, corresponding to a rapid increase in green density with pressing pressure. The gradients of 14 and 16 were comparable to gradients obtained by Theunissen for laboratory-synthesized Y-TZP powders prepared by chloride and alkoxide routes [13] and Samdi *et al.* for Y-TZP powders prepared from acetate solutions [14]. Powder C and commercial TZ-2Y [13]. Fig. 3b, produced gradients of ~7 and ~9, respectively.

A change in the slope of the compaction curve would indicate the breakdown of soft agglomerates [15–17], but no such change was observed with any of the three powders (Powders A–C). It is possible that the agglomerates broke down at compaction pressures lower than those used in this study (20–140 MPa), as previous workers have observed such agglomerate breakdown with compaction pressures in the range 5–40 MPa [13, 14, 18].

Increasing the compaction pressure up to 150 MPa did not result in an improvement of the maximum sintered densities observed for Powders A, B and C, upon the values obtained using a compaction pressure of 80 MPa, Section 3.2.1. It has been reported that the compaction behaviour of agglomerated powder is related to its sinterability; if the agglomerates are softly bonded and can be broken down by compaction, the sinterability will be unaffected by agglomeration [18]. Hard agglomerates, however, may not be broken

down by compaction and the sinterability may be poor.

3.2.3. Dilatometry

Dilatometry was used to investigate the sintering behaviour of compacted Powders A, B and C. The shrinkage curves for Powders A, B and C were similar and the powders appeared to have fully densified by 1500 °C.

The different sintering behaviour of Powders A, B and C was further illustrated by comparing the temperature at which the maximum rate of densification, max. dL/dt, occurred, Table II. The temperature at which the max. dL/dt occurred was determined from the rate of shrinkage curve dL/dt versus temperature. Powder B again produced different results, with a maximum densification temperature which was 30–40 °C higher than for Powders A and C.

The activation energies for the sintering of the different powders were determined using data obtained from the dilatometry experiments. The densification of a compacted powder during the initial stage of sintering can be described by Equation 1

$$\left[\frac{(\Delta l/l_0)}{T}\right] = \text{const. } \exp\left(\frac{-nE_A}{RT}\right) \quad (1)$$

where $\Delta l/l_0$ is the relative shrinkage at temperature T, E_A is the activation energy and n is a constant describing the transport path for material transfer ($n = 1$, $\frac{1}{2}$ and $\frac{1}{3}$ for viscous, volume and grain-boundary diffusion, respectively) [19]. Assuming grain-boundary diffusion [19–21], $n = \frac{1}{3}$, the activation energies were obtained by plotting $\ln[(\Delta l/l_0)T]$ against $1/T$, producing a slope of $-nE_A/R$. Table II lists the activation energies of Powders A, B and C calculated using the data from the linear region of 5–15% shrinkage.

Powders A and C had similar activation energies of sintering (615 and 605 kJ mol^{-1} respectively), whereas Powder B had a slightly larger activation energy (645 kJ mol^{-1}). Lawson obtained values of $\sim$490 and 570 kJ mol^{-1} for two commercial Y-TZP powders (Tioxide 2.5 mol % Y-TZP and Tosoh 3 mol % Y-TZP, respectively) using the above method [20]. Gupta *et al.* calculated an activation energy of 610 kJ mol^{-1} for TZP ceramics by plotting the reciprocal time required to reach peak density versus $1/T$ [22]. Other values reported for various yttria–zirconia powders, also assuming grain-boundary diffusion, range from 275 kJ mol^{-1} [21] to 540 kJ mol^{-1} [23].

TABLE II Temperatures of max. dL/dt and activation energy of sintering for Powders A, B and C obtained from dilatometry analysis

Sample	Temp. (°C) of max. dL/dt	Activation energy (kJ mol^{-1})
Powder A	1338	615
Powder B	1377	645
Powder C	1341	605

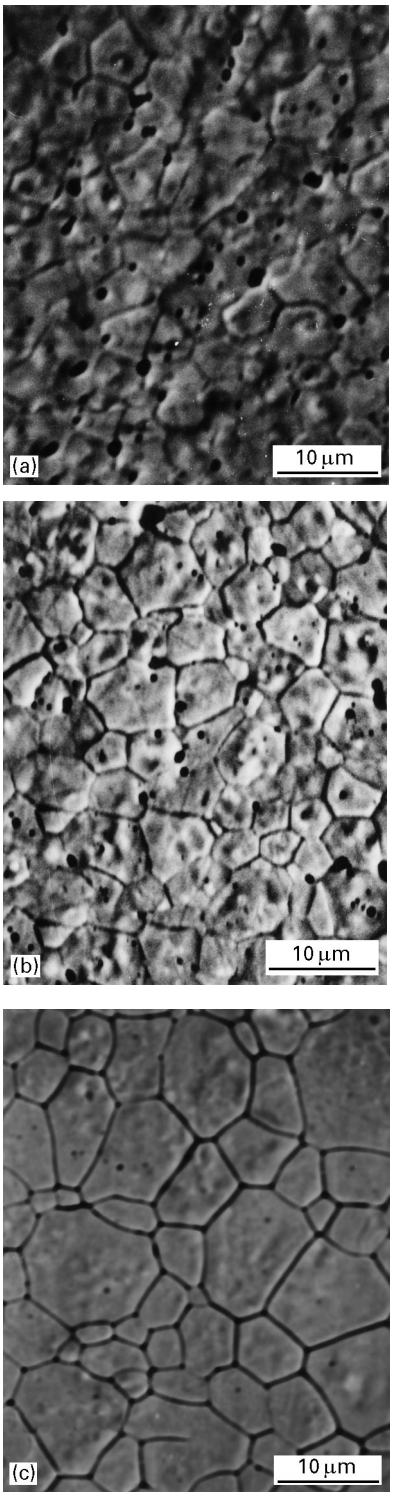

Figure 4 Scanning electron micrographs of sintered ceramics produced from (a) Powder A, (b) Powder B and (c) Powder C. Samples were sintered at 1500 °C for 2 h.

The sinterability of Powders A and C were comparable. Although Powder A had the highest surface area and the narrowest powder particle size distribution of all three powders in this study, the sintered ceramic produced from Powder C had the highest sintered density. The onset of densification was similar for Powder A and C; this was also reflected by the results from the dilatometry experiments. In comparison, the sinterability of Powder B was significantly poorer than Powders A and C; however, the maximum sintered density of A and B were comparable, at

$\sim$98% at 1500 °C. Although the highly irregular-shaped powder particles and wide particle-size distribution affected the temperature at which Powder B densified and its activation of sintering, its poorer powder characteristics did not appear significantly to affect the maximum sintered density.

A significant point to note when comparing the sintered densities is that the same value of theoretical density was used for all ceramics prepared from the three powders; the theoretical density was determined from crystallographic data of YSZ [9]. However, Powder C contains a small level of hafnia (approximately 2 wt % HfO_2), whereas Powders A and B do not contain hafnia. This may have the effect of overestimating the percentage theoretical density of ceramics prepared from Powder C by up to 1.4%.

Powders A and B were prepared by similar routes [8, 24] and consisted of unreacted monoclinic zirconia and yttria, unlike Powder C which was almost 100% cubic yttria-stabilized zirconia. The sintering of Powders A and B, therefore, also involves the reaction of the monoclinic zirconia and yttria to produce cubic yttria-stabilized zirconia. As these two powders have very different powder characteristics but produce very similar sintered densities, it is likely that the zirconia/yttria reaction is more significant in determining the maximum sintered densities of Powders A and B.

Another guide to the differences observed in the maximum sintered densities between Powders A and B ($\sim$98%) and Powder C (99.5%) is the values of m obtained from the compaction curves of green density versus log (compaction pressure) plots. Powder C had a low value of m ($\sim$7) compared to the high values of $\sim$14 and $\sim$16 for Powders A and B, respectively. Higher values of m suggest the presence of hard agglomerates. Although Powders A and C appeared to be very similar from SEM and particle-size analysis, the agglomerates of small crystallites which make up the spherical powders particles observed in Fig. 1a and c may be much harder in Powder A than in Powder C. Powder B has a comparable value of m to Powder A and both powders produce ceramics with similar densities.

3.2.4. SEM

The microstructures of sintered samples were examined using SEM. Fig. 4a–c shows the typical microstructures of ceramics prepared from Powders A, B and C which were sintered at 1500 °C for 2 h. Powder C, Fig. 5c, appeared to produce a very dense ceramic; only a small number of trapped pores were observed. The ceramics produced from Powders A and B had smaller grain sizes than ceramics from Powder C, but both samples had significantly higher levels of porosity, with pores existing within grains and along grain boundaries/triple points. The average grain sizes are listed in Table III.

Although ceramics produced from Powder B had the lowest sintered density, the average grain size was the smallest of all three materials. The ceramic produced from Powder C had the largest average grain size but also had the highest sintered density. The sintering schedule used, 1500 °C for 2 h, probably resulted in significant grain growth for ceramics prepared from Powder C. A sintering schedule involving a sintering dwell of only 1 h at 1500 °C resulted in a decrease in the average grain size for ceramics prepared from Powder C to only 6 μm [25].

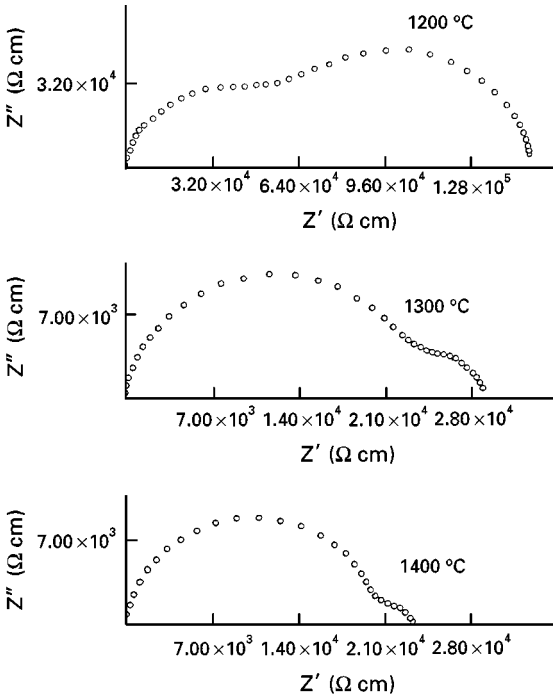

Figure 5 A.c. impedance plots, $-Z''$ versus Z, obtained at 365 °C for samples produced from Powder C sintered at (a) 1200, (b) 1300 and (c) 1400 °C, producing densities of 71%, 92.5% and 97%, respectively.

3.2.5. Conductivity measurements

A.c. impedance spectroscopy has been used to study the effect of microstructure, grain size and porosity on the electrical properties of stabilised zirconia [26]. The porosity is believed to affect the grain-boundary resistance and the bulk resistance remains unchanged; this was illustrated by Badwal and Drennan [6], who used a pre-reacted 10 mol % YSZ and measured the conductivity for sintering temperatures between 1300 and 1900 °C. Schouler *et al.*, however, observed a change in bulk resistance with sintering temperature and porosity, using an unreacted 10 mol % YSZ [5].

Fig. 5 shows impedance plots obtained at 365 °C for samples produced from Powder C sintered at 1200, 1300 and 1400 °C, producing densities of 71%, 92.5% and 97%, respectively. The impedance plots were collected at 365 °C as this temperature allows the bulk and grain-boundary components of the resistance to be clearly separated and their values calculated [11]. For low sintering temperatures, two poorly resolved semicircles were observed and increasing the sintering temperature improved the separation of the two semicircles.

The bulk resistance, measured at 365 °C, decreased with increasing sintering temperature/density, Fig. 6a, and reached a constant value above $\sim$1300 °C; the bulk capacitance remained essentially constant for all

TABLE III Average grain sizes of ceramics prepared from Powders A, B and C, sintered at 1500 °C for 2 h

Sample	Average grain size (μm)
Powder A	9
Powder B	8
Powder C	11

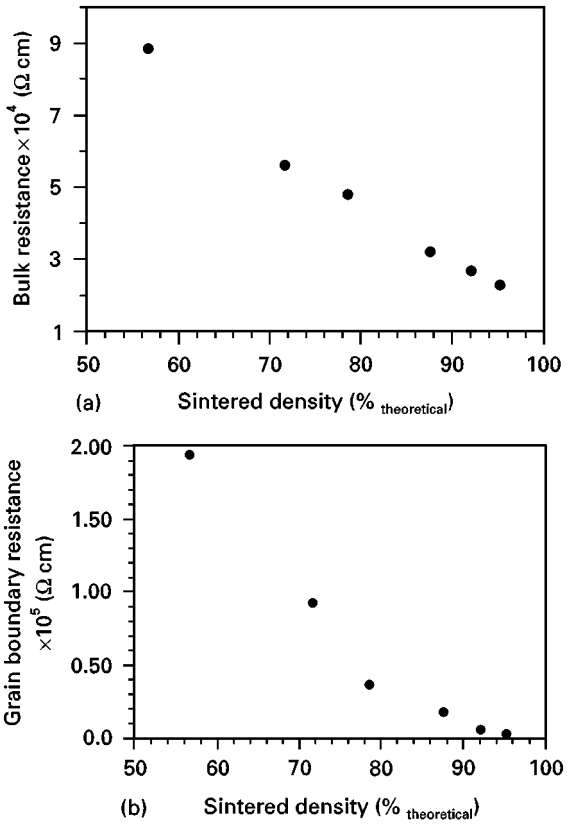

Figure 6 The effect of sintered density on (a) bulk resistance and (b) grain-boundary resistance, measured at 365 °C, of samples prepared from Powder C.

sintering temperatures. The grain-boundary resistance decreased significantly with increasing temperature/density, Fig. 6b, again remaining relatively constant above ~1300 °C. The grain-boundary capacitance increased by two orders of magnitude between 1200 and 1500 °C indicating improved sintering [11]. The small grain-boundary capacitance observed for low sintering temperatures led to the poor resolution of the bulk and grain-boundary semicircles observed for samples sintered at 1200 °C. For samples sintered at low temperatures, the time constants (RC) of the bulk and grain-boundary components were of comparable magnitude, whereas for samples sintered at high temperatures the time constants are separated by two orders of magnitude. The sintering temperature at which no significant change in bulk and grain-boundary resistance was observed, ~1300 °C, corresponded closely to the results obtained in Section 3.2.1, where Powder C had reached an approximately constant density at ~1300 °C.

Similar results were observed for samples prepared from Powder A sintered at temperatures between 1200 and 1500 °C, with changes in bulk and grain-boundary resistance observed below ~1300 °C but constant values obtained above ~1300 °C.

The correlation between porosity and conductivity has been investigated by Inozemtsev *et al.* [27] using scandia-stabilized zirconia. For porosity between ~5% and 25%, where per cent porosity was assumed to be (100%-density), the conductivity was found to decrease linearly with increasing porosity [28].

The dependence of R_{GB}/R_{TOTAL} upon porosity and sintering temperature has been studied. The contribution of the grain-boundary resistance to the total resistance varied with porosity/sintering temperatures. For porosity greater than ~5%, the contribution of the grain-boundary resistance to the total resistance exceeded 15% at 365 °C. Sintering temperatures greater than 1300 °C were therefore required to obtain an acceptably low grain-boundary contribution of 10%–15%. R_{GB}/R_{TOTAL} is seen to vary approximately linearly with increasing porosity between 2% and 30%, Fig. 7a.

R_{GB}/R_{TOTAL} has previously been parameterized as α_R, or the blocking effect [4, 27, 29] where

$$\alpha_R = \alpha_{GB}/\alpha_{TOTAL} = (R_{GB}/R_{TOTAL})^{-1} \quad (2)$$

α_R is plotted against porosity and sintering temperature in Fig. 7b and c. As the contribution of the grain-boundary resistance to the total resistance decreases, α_R increases; low porosity yields high values of α_R and increasing porosity produces a steady decrease in α_R.

The poor resolution of the semicircles in the impedance plots obtained for porous samples makes identification of components and subsequent measurement difficult.Using a.c. impedance spectroscopy, a contribution from the porosity to the impedance plot has been proposed [7, 30]. The contribution consisted of a small semicircle positioned between the high-frequency bulk semicircle and the lower frequency grain-boundary semicircle. Using an a.c. impedance curve fitting program by Boukamp (EQUIVALENT CIRCUIT) [31], an additional semicircle could not be identified in impedance plots of samples prepared from Powders A or C sintered at 1200 °C. The absence of an additional semicircle indicated that the effect of the high porosity was manifested in the grain-boundary semicircle and did not contribute separately to the impedance plot. In support of the observations of Kleitz *et al.* [30] and Dessemond *et al.* [7], the higher values of bulk resistance observed at sintering temperatures below 1300 °C may indicate the presence of an additional component. For sintering temperatures >1300 °C, the bulk resistance remained constant which could indicate the disappearance of any additional semicircle.

Provided that YSZ can be sintered to >95% theoretical density, the effect of the porosity on the bulk and grain-boundary conductivity will be minimal. For Powders A, B and C, sintering temperatures >1300 °C were required to obtain this lower limit of sintered density.

Recent reviews of commercially available 8 mol % YSZs reported their densities after sintering at 1500 °C

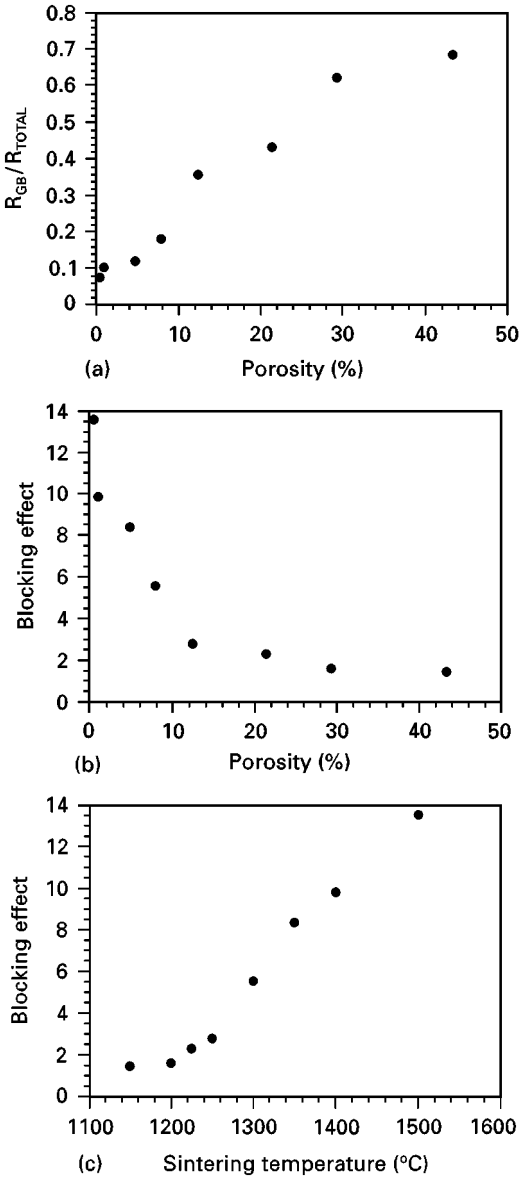

Figure 7 The effect of porosity/sintering temperature on the contribution of the grain-boundary resistance to the total resistance, for data obtained at 356 °C, plotting (a) R_{GB}/R_{TOTAL} against porosity, (b) $\alpha_R(= R_{TOTAL}/R_{GB})$ against porosity and (c) α_R against sintering temperature.

for 1 h [32] and 1500 °C for 4 h [33] and the conductivity of the various samples at 1000 °C. A selection of these results are listed in Table IV, along with the data obtained for samples prepared from Powder A, B and C.

A range of conductivity values was obtained from the different studies and the variations were probably due to density variations and the different experimental set-ups used to measure the conductivity; variations in grain size, sample purity and absolute yttria content may also be responsible. For example, Table IV shows the sintered density and conductivity data for the same material (Tosoh TZ-8Y), but measured by three different groups and producing three different results. It is clear from the results listed in Table IV, however, that varying the density, even above 95%, can produce variations in the conductivity at 1000 °C.

Although ceramics produced from Powders A and B had slightly lower sintered densities than from Powder C, the difference was very small (1%–2%) and the conductivities at 1000 °C, the recognized SOFC operating temperature, were comparable. This study highlights the ability to produce yttria–stabilized zirconia powders by novel synthesis routes which result in ceramics with comparable sinterability and electrical properties to widely accepted commercial YSZ materials.

TABLE IV Sintered densities and conductivities of commercial 8 mol % YSZs

Company	Density (%)	Conductivity ($S\,m^{-1}$)	Ref.
Mitsibushi	96.5	13	[32]
Degussa	97	14.5	[32]
Lonza	95.6	15	[32]
Tosoh TZ-8Y	97.5	14	[32]
Daiichi	99.5	17.7	[33]
Nissan Chemical Co.	99.2	17.8	[33]
Scimarec Co.	97.7	16.5	[33]
Tosoh TZ-8Y	99.3	17.1	[33]
Powder A	98.5	15.5	Present work
Powder B	98.2	16.0	Present work
Powder C	99.7	15.6	Present work

4. Conclusion

The powder characteristics, such as surface area and particle size, of Powders A and C are comparable. By contrast, Powder B has a very small surface area and a very wide particle-size distribution. This reflects the fact that the production of Powders A and C involved a spray-drying step whereas Powder B was not spray-dried.

The densities of a YSZ prepared by a coating technique (Powder A) and a YSZ prepared by a co-milling technique (Powder B), sintered at 1500 °C for 2 h, are 98.5% and 98.2%, respectively. A co-precipitated YSZ (TZ-8Y), Powder C, has a sintered density of 99.7%. From dilatometry analysis, Powders A, B and C have similar activation energies, calculated for a relative shrinkage of 5%–15%. Powder B has a slightly higher activation energy of sintering than the other two powders.

SEM analysis shows that sintered ceramics prepared from Powder C have a bimodal grain-size distribution and has the largest average grain size of the three materials. Sintered ceramics of Powders A and B have similar, unimodal grain-size distributions. A higher level of porosity is observed in ceramics of Powder A and B than in Powder C.

The bulk and grain-boundary conductivity of YSZ samples prepared from Powders A and C remain unchanged for sintered densities between 95% and 100%. Lower sintered densities produce a small decrease in bulk conductivity and a large decrease in grain-boundary conductivity. The sintered density and the ionic conductivity at 1000 °C of samples prepared from Powders A and B are comparable to values reported for a variety of commercially available 8 mol % YSZs.

Acknowledgements

The authors gratefully acknowledge Tioxide Specialties Ltd and the University of Aberdeen for funding (IG).

References

1. J. H. HIRSCHENHOFER, *IEEE Aerospace Electron Systems Mag.* **12** (1997) 23.
2. R. J. BROOK, in "Advances in Ceramics", Vol. 3, edited by A. H. Heuer and L. W. Hobbs (The American Ceramic Society, Columbus, OH, 1981) p. 272.
3. T. OKUBO and H. NAGAMOTO, *J. Mater. Sci.* **30** (1995) 749.
4. M. KLEITZ, H. BERNARD, E. FERNANDEZ and E. SCHOULER, in "Advances in Ceramics", Vol. 3, edited by A. H. Heuer and L. W. Hobbs (The American Ceramic Society, Columbus, OH, 1981) p. 310.
5. E. J. L. SCHOULER, N. MESBAHI and G. VITTER, *Solid State Ionics* **9**/**10** (1983) 989.
6. S. P. S. BADWAL and J. DRENNAN, *J. Mater. Sci.* **22** (1987) 3231.
7. L. DESSEMOND, J. GUINDET, A. HAMMOU and M. KLEITZ, in "Proceedings of the 2nd International Symposium on SOFC's", edited by F. Grosz, P. Zegers, S. C. Singhal and O. Yamamoto (Office for Official Publications of the European Communities, Brussels, Belgium, 1991) 409
8. G. P. DRANSFIELD, K. A. FOTHERGILL and T. A. EGERTON, in "Euro-ceramics", Vol. 1, edited by G. de With, R. Terpstia and R. Metselaar (Elsevier, London, 1989) p. 275.
9. PDF Card no. 30-1468, ICDD, Newton Square, A, USA (1980).
10. M. I. MENDELSON, *J. Am. Ceram. Soc.* **52** (1969) 443.
11. J. T. S. IRVINE, D. C. SINCLAIR and A. R. WEST, *Adv. Mater.* **2**(3) (1990) 132.
12. K. MASTERS, *Am. Ceram. Soc. Bull.* **73**(1) (1994) 63.
13. G. S. A. M. THEUNISSEN, PhD thesis, University of Twente, Enschede, The Netherlands, (1991).
14. A. SAMDI, B. DURAND, M. ROUBIN, A. DAOUDI, M. TAHA, J. PALETTO and G. FANTOZZI, *J. Eur. Ceram. Soc.* **12** (1993) 353.
15. M. A. C. G. van de GRAAF, J. H. TER MAAT and A. J. BURGGRAAF, *J. Mater. Sci.* **20** (1985) 1407.
16. A. ROOSEN, *Adv. Ceram. Mater.* **3**(2) (1988) 131.
17. D. E. NIESZ, R. B. BENNET and M. SNYHDER, *Am Ceram. Soc. Bull.* **51** (1972) 677.
18. J. L. SHI, Z. X. LIN, W. J. QIAN and T. S. YEN, *J. Eur. Ceram. Soc.* **13** (1994) 265.
19. W. S. YOUNG and I. B. CUTLER, *J. Am. Ceram. Soc.* **53** (1970) 659.
20. S. LAWSON, PhD thesis, University of Sunderland (1993).
21. G. S. A. M. THEUNISSEN, A. J. A. WINNUBST and A. J. BURGGRAAF, *J. Eur. Ceram. Soc.* **11** (1993) 315.
22. T. K. GUPTA, *Sci. Sint.* **10** (1979) 205.
23. D. D. UPADHYAYA, T. R. G. KUTTY and C. GANGULY, in "Science and Technology of Zirconia V" edited by S. P. S. Badwal, M. J. Bannister and R. H. J. Hannink (Technomic, Lancaster, PA, USA, 1993) p. 310.
24. I. R. GIBSON, E. E. LACHOWSKI, J. T. S. IRVINE and G. P. DRANSFIELD, *Solid State Ionics* **72** (1994) 265.
25. I. R. GIBSON, G. P. DRANSFIELD and J. T. S. IRVINE, *J. Eur. Ceram. Soc.* **18** (1998) 661.
26. J. A. KILNER and B. C. H. STEELS, in "Non-stoichiometric Oxides", edited by O. T. Sørensen (Academic Pres, New York 1981) p. 233.
27. M. V. INOZEMTSEV, M. V. PERFIL'EV and A. S. LIPILIN, *Elektrokhimiya* **10** (1974) 147.
28. M. J. VERKERK, B. J. MIDDELHUIS and A. J. BURGGRAAF, *Solid State Ionics* **6** (1982) 159.
29. H. BERNARD, PhD thesis, Grenoble, France (1980).
30. M. KLEITZ, C. PESCHER and L. DESSEMOND, in "Science and Technology of Zirconia V, edited by S. P. S. Badwal, M. J. Bannister and R. H. J. Hannink (Technomic, Lancaster, PA, USA, 1993) p. 593.
31. B. BOUKAMP, *Equivalent Circuit* Ver 3.99, University of Twente, The Netherlands (1992).
32. R. MAENNER, E. IVERS-TIFFÉE, W. WERSING and W. KLEINLEIN, in "Proceedings of the 2nd International Symposium on SOFC's", edited by F. Grosz, P. Zegers, S. C. Singhal and O. Yamamoto (Office for Official Publications of the European Communities, Brussels, Belgium, 1991) 409
33. F. T. CIACCHI, K. M. CRANE and S. P. S. BADWAL, *Solid State Ionics* **73** (1994) 49.

Received 20 April
and accepted 15 May 1998